9

Analysis of Dynamic Optical Imaging Data

PARTHA P. MITRA, BIJAN PESARAN, AND DAVID KLEINFELD

INTRODUCTION

Dynamic optical imaging data generate large data sets that contain signal and noise components of considerable spatiotemporal complexity. Advances in available computational power now make it possible to identify and remove noise components and characterize signal structure using modern signal and image processing techniques.

Noise in imaging data arises from two broad categories of sources, biological and nonbiological. Biological sources like cardiac and respiratory cycles are routinely present, as well as motion of the experimental subject and slow vasomotor oscillations (Mayhew et al. 1996; Mitra et al. 1997). In all studies of evoked activity, ongoing brain activity not locked to or triggered by the stimulus is another source of biological noise. Nonbiological noise sources in imaging experiments include photon-counting statistics, electronic instrumentation, 60 Hz electrical activity, CCD camera refresh-rates, and building vibrations, to name a few. All of this activity combines to mask the neuronal signals of interest.

This chapter presents applications of modern signal and image processing techniques that have proven useful for optical imaging data with both intrinsic and extrinsic sources of contrast. The main tools are drawn from multitaper spectral analysis, harmonic analysis, and, when dealing with multivariate data (the usual situation in imaging experiments), the singular value decomposition (SVD).

MATHEMATICAL METHODS

Three tools for the analysis of optical imaging data are presented below: multitaper spectral estimation, harmonic analysis, and the SVD in two different forms. This presentation is focused on the use of the tools rather than on their derivation. Further information on the technical aspects of the discussion is available in the following references (Thomson 1982; Percival and Walden 1993; Mitra and Pesaran 1999).

Multitaper Spectral Estimation

Spectral estimation is based on the premise that the frequency domain is the appropriate basis in which to examine dynamic activity. This assumes that the activity is stationary. Although this is not usually true of neural activity on long time scales, say hours, it is not unreasonable to suggest that on a subsecond time scale neural processes change very little. The approach is to then repeat the calculation on neighboring windows overlapping in time, usually displaced by a fixed amount. The result is a time-frequency representation of the function being calculated.

Conventional spectral analysis involves multiplying time series data by a single taper (conventionally known as a window). Examples of such single tapers are Hamming, Hanning, and Cosine tapers. We use multitaper methods in which many tapers are used to operate on a single window in time of the data. The tapers used are the Slepian functions, or discrete prolate spheroidal sequences (DPSS), which form a set of orthogonal functions. The Slepian functions are characterized by a single parameter W also called the "bandwidth" parameter. This parameter specifies the frequency and bandwidth of the Slepian functions. For a given frequency half-bandwidth W and length N, there are approximately $2NW$ Slepian functions $w_k(t)$ ($k = 1..[2NW]$, $t = 1..N$) that have their spectra well concentrated in the frequency range $[-W, W]$.

Step 1: Computing the Slepian Functions

The Slepian functions are characterized by their length N and bandwidth parameter W, and routines exist on the web to calculate them (see WWW site at http://www.vis.caltech.edu/~WAND/wand98/bijan.html) using the LAPACK library of linear algebra routines. The routines are also available in Matlab 5.0 or later, see routines **dpss** and **pmtm**. The parameters N and W determine the maximum number of functions usable, $K = [2NW]$, and their selection is up to the judgment of the investigator based on a knowledge of the dynamics of the processes under investigation. This choice is then best made iteratively by visual inspection and some degree of trial and error. $2NW = 2W/(1/N)$ gives the number of effectively independent frequencies over which the spectral estimate is smoothed, so that the variance in the estimate is typically reduced by $2NW$. Thus, the choice of W is a choice of how much to smooth. As a rule of thumb, we find that fixing the time bandwidth product NW at a small number (typically 3 or 4) and then varying the window length in time until sufficient spectral resolution is obtained is a reasonable strategy.

Step 2: Computing the Tapered Fourier Transforms

The next step is the computation of the tapered Fourier transforms of the data x_t ($t = 1, \ldots, N$) for each taper $w_t(k)$ ($k = 1, \ldots, K$)

$$\tilde{x}_k(f) = \sum_{t=1}^{N} w_t(\mathrm{k}) x_t e^{-2\pi i f t} \tag{1}$$

Step 3: Direct Spectral Estimate

The simplest example of the multitaper method is given by the direct multitaper spectral estimate $S_{MT}(f)$, obtained as the average over individual windowed spectral estimates,

$$S_{MT}(f) = \frac{1}{K}\sum_{k=1}^{K}\left|\tilde{x}_k(f)\right|^2 \tag{2}$$

The spectrum may be computed with a moving window to obtain a spectrogram, which provides a time-frequency representation of the data.

Harmonic Analysis

Multitaper methods provide a robust and efficient way to carry out harmonic analysis: the analysis of discrete sinusoidal components of activity present in a continuous background. This allows the detection, estimation of parameters, and extraction of the sinusoidal activity on a short moving window.

An optimally sized analysis window is needed. This window must be sufficiently small to capture the variations in the amplitude, frequency, and phase, but long enough to have the frequency resolution to separate the relevant peaks in the spectrum, both artifactual and originating in the desired signal.

Step 1: Detection and Estimation of a Sinusoid in a Colored Background

The presence of a sinusoidal component in colored noise background may be detected by a test based on a goodness of fit F-statistic (Thomson 1982). The activity is modeled on a sinusoid of frequency f with a certain amplitude and phase added to a random noise process which is locally white on a scale given by the bandwidth parameter W of the tapers.

$$a(t) = \sum_n A_n \cos[f_n t + \phi_n] + \delta a(t) \tag{3}$$

Using the tapered Fourier transforms of the data, $x_k(f)$, an estimate of the amplitude A_n and phase ϕ_n is given by the complex amplitude, $\mu_n(f_n)$ of the sine wave

$$\hat{\mu}_n(f_n) = \frac{\sum_k x_k(f_n)U_k(0)}{\sum_k \left|U_k(0)\right|^2} \tag{4}$$

$$\hat{\mu}_n(f_n) = \frac{A_n e^{i\phi_n}}{2} \tag{5}$$

The goodness of fit F-statistic which allows us to test the hypothesis that the sine wave is present at that frequency is given by

$$F(f_n) = \frac{(K-1)\left|\hat{\mu}_n(f_n)\right|^2 \sum_k \left|U_k(0)\right|^2}{\sum_k \left|\tilde{x}_k(f_n) - \hat{\mu}_n(f_n)U_k(0)\right|^2} \tag{6}$$

The quantity in Equation 6 is F-distributed with (2,2*K*–2) degrees of freedom. The significance level is chosen to be 1–1/N so that on average there will be one false detection of a sinusoid across all frequencies.

If the cause of the estimated sinusoid is considered to be noise, one may subtract it from the data, and the spectrum of the residual time series may be obtained as before.

Step 2: Removal of Periodic Components

The parameters A_n, f_n, and ϕ_n are estimated as a function of time by using a moving time window. The goal is to estimate the smooth functions, $A_n(t)$, $f_n(t)$, and $\phi_n(t)$, that give the component to be subtracted from the original time series.

The frequency F-test described above is used to determine the fundamental frequency tracks $f_n(t)$ in Equation 3. The time series used for this purpose may either be a single time series in the data or an independently monitored physiological time series. The fundamental frequency tracks are used to construct the tracks for the harmonics and sums and differences of individual oscillations, usually respiration and cardiac rhythms, generated by interactions between them. The final set $f_n(t)$ contains all these frequency tracks.

The estimated sinusoids are reconstructed for each analysis window, and the successive estimates are overlap-added to provide the final model waveform for the artifacts. If more precision is required, the estimates for the amplitude and phase for each window can be spline-interpolated to each digitization point to allow for nonlinear phase changes over the shift between each window. This is akin to using a shift in time between two successive analysis windows of the sampling rate, but is achieved at far less computational cost.

Multivariate Time-series Methods

To this point, the operations have been described on univariate data, but optical imaging data consist of many pixels of activity that are recorded simultaneously and lead to multivariate time series.

The SVD is a general matrix decomposition of fundamental importance that is equivalent to principal component analysis in multivariate statistics, but also generates low-dimensional representations for complex multidimensional time series. Consequently, the SVD is a powerful tool both to reduce the number of interesting dimensions of the data and to characterize coherent states of activity. Routines to compute the SVD of a general matrix are widely available as part of linear algebra packages

such as LAPACK or as part of general data analysis software such as IDL (Research Systems) and MATLAB (Mathworks).

We present two applications of the SVD, one to imaging data in its more usual space and time dimensions, the space-time SVD, and one when we have Fourier-transformed the time dimension into frequency to give the space-frequency SVD.

Space-time SVD

The space-time SVD is a one-step operation on the space-time data $I(\mathbf{x}, t)$. The SVD of such data is given by

$$I(\mathbf{x},t) = \sum_n \lambda_n I_n(\mathbf{x}) a_n(t) \tag{7}$$

where $I_n(\mathbf{x})$ are the eigenmodes of the "spatial correlation matrix." Similarly $a_n(t)$ are the eigenmodes of the "temporal correlation matrix" (Mitra and Pesaran 1999). The values of λ_n give the amount of power or variance in each of the ordered space and time eigenmodes. Their relative values give an indication of how large the signal is compared to the noise and allow data dimension reduction for the purposes of visual inspection.

Applications of the SVD on space-time imaging data are abundant in the literature. However, the space-time SVD suffers from a severe drawback in the present context because there is no reason the neurobiologically distinct modes in the data should be orthogonal to each other, a constraint imposed by the SVD. In practice, it is observed that on performing an SVD on space-time data, different sources of fluctuations may appear in the same mode of the decomposition, thus preventing segregation of the activity.

In the next section, a more effective way of separating distinct components in the data using a decomposition analogous to the space-time SVD, but in the space-frequency domain, is presented. The success of the method stems from the fact that the data in question are better characterized by a frequency-based representation.

Space-frequency SVD

The basic idea is to project the space-time data to a frequency interval, and then perform an SVD on this space-frequency data (Thomson and Chave 1991; Mann and Park 1994; Mitra et al. 1997). Projecting the data on a frequency interval can be performed effectively by using DPSS with the appropriate bandwidth parameter.

Step 1: Constructing the space-frequency matrix. Given the $N_x \times N$ space-time data matrix $I = I(x, t)$, the space-frequency data corresponding to the frequency band $[f - W, f + W]$ are given by the $N_x \times K$ complex matrix

$$\tilde{I}(x,k;f) = \sum_{t=1}^{N} I(x,t) w_k(t,W) e^{2\pi i t f} \tag{8}$$

Step 2: SVD of the space-frequency matrix. We are considering here the SVD of the $N_x \times K$ complex matrix with entries $\tilde{I}(x,k;f)$ for fixed f.

$$\tilde{I}(x,k;f) = \sum_n \lambda_n(f)\tilde{I}_n(x;f)a_n(k;f) \tag{9}$$

This SVD can be carried out as a function of the center frequency f, using an appropriate choice of W. At each frequency f, one obtains a singular value spectrum $\lambda(f)$ (n = 1,2,..,K), the corresponding (in general complex) spatial mode $\tilde{I}_n(x;f)$, and the corresponding local frequency modes $\tilde{a}_n(k;f)$. The frequency modes can be projected back into the time domain to give (narrowband) time-varying amplitudes of the complex eigenimage. For details of this reconstruction, see Mann and Park (1994).

Step 3: A measure of spatial coherence. In the space-frequency SVD computation, an overall coherence $\bar{C}(f)$ may be defined as (it is assumed that $K \leq N_x$)

$$\bar{C}(f) = \frac{\lambda_1^2(f)}{\sum_{n=1}^{K} \lambda_n^2(f)} \tag{10}$$

The overall coherence spectrum then reflects how much of the fluctuation in the frequency band $[f - W, f + W]$ is captured by the dominant spatial mode. The value ranges between 0 and 1 and for random data $\bar{C}(f) \sim \frac{1}{K}$, which sets a threshhold for significance.

EXPERIMENTAL METHODS

We present an application of the above tools to optical imaging data from rat somatosensory cortex. In this data set, the cortex was stained with a voltage-sensitive dye, and we consider the changes in fluorescence as a function of time (see Chapters 49 and 50).

The subject was a male Sprague-Dawley rat with a mass of 58 g. The animal was prepared and maintained as described previously (Kleinfeld and Delaney 1996). An approximately 4 x 4-mm region of the primary vibrissa areas of parietal cortex was stained, following microdissection of the dura, with the dye RH-795 (Molecular Probes). A metal frame was fixed to the skull that surrounded the craniotomy as a means to rigidly hold the head of the animal to the optical apparatus. With the addition of agarose gel and a coverglass window, this frame further served as an optically clear chamber that sealed and protected the cortex (Kleinfeld and Delaney 1996); resealing the craniotomy was crucial for the mechanical suppression of excessive motion that would otherwise result from changes in cranial pressure with each heart beat and breath.

We recorded the fluorescent yield from the cortical surface with a CCD camera (no. PXL 37; Photometrics), from which the signal was calculated as the change in fluorescence relative to the background level. The pixel field was 30 x 90, the sampling rate was 95.4 Hz, and records were 3000 frames (286 sec) in length. Each pixel represents an estimated 300,000 electrons, so the sensitivity per pixel per sample was limited to a fractional change of approximately 0.002. The EKG and breathing were further recorded. No stimuli were applied to the rat during data acquisition. Note that the voltage-

sensitive dye fluorescence reports intrinsic changes in the optical properties of cortex (Grinvald et al. 1986; Kleinfeld and Delaney 1996), including those related to hemodynamics.

DATA ANALYSIS STRATEGY

In this section, we present an application of the above tools to the intrinsic component of the optical imaging data from the rat somatosensory cortex. There are two stages to the analysis, exploratory and confirmatory. Exploratory analysis determines parameters of interest and the structure of any noise present. The noise is then filtered and the signal structure is characterized.

Step 1: Visualization of the Raw Data

Direct visualization of the raw data is the first step to check the quality of the experiment and direct further analysis. Individual time series from the images and movies of the images should be examined.

If the images are noisy, e.g., due to large shot noise, truncation of a space-time SVD with possibly some additional smoothing provides a simple noise-reduction step for the visualization.

A space-time SVD of the data is first computed, followed by sinusoidal modeling of the leading principal component time series (Figure 9.1). This is useful for two reasons: (1) The images in question typically have many pixels, and it is impractical to perform the analysis separately on all pixels. (2) The leading SVD modes capture a large degree of global coherence in the oscillations. However, the procedure may as well be applied to individual image time series.

Step 2: Preliminary Characterization

The next stage aims to identify the various artifacts and determine a preliminary characterization of the signal. A time-frequency spectral estimate described above should be calculated (Figure 9.1B). This can be done on individual pixels, or a space-time SVD can be first calculated followed by operations on the leading principal components.

A more powerful characterization is obtained by the space-frequency SVD (Figure 9.2). There is sufficient frequency resolution in optical data so that the oscillatory artifacts segregate well. Studying the overall coherence spectrum reveals the degree to which the images are dominated by the respective artifacts at the relevant frequencies, while the corresponding leading eigenimages show the spatial distribution of these artifacts more cleanly compared to the space-time SVD (Figure 9.2). Moreover, provided the stimulus response does not completely overlap the artifact frequencies, a characterization is also obtained of the spatiotemporal distribution of the stimulus response.

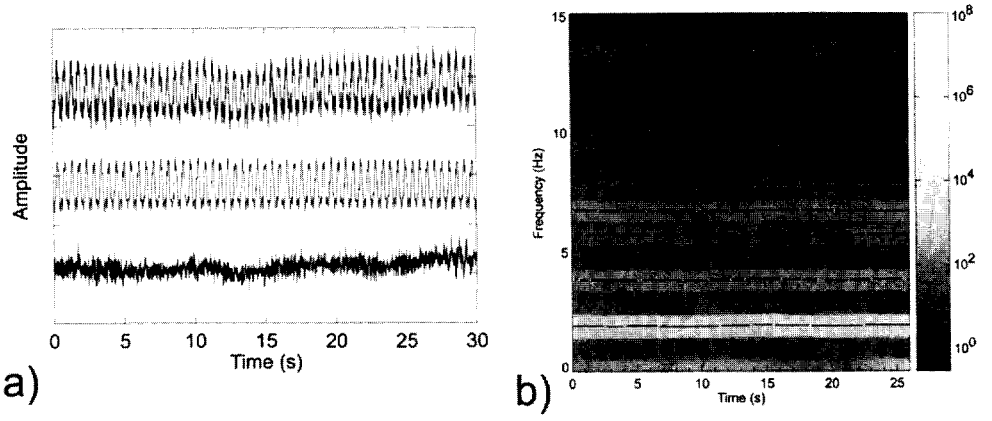

Figure 9.1. Optical imaging data from rat somatosensory cortex. (*a*) Noise suppression of cardiac and respiratory rhythms. The figure shows the results of filtering the respiratory and cardiac rhythms from a single principal component mode in the time domain. The top curve is the raw mode. The middle curve shows the reconstructed noise signal using the overlap-add technique described in the text. The bottom curve shows the residual signal after noise suppression. (*b*) Time-frequency representation of the raw mode from the top of part *a*. The black lines show the estimated frequency tracks. The fundamental of the respiratory rhythm was at 1.5 Hz and that of the cardiac rhythm at 7 Hz.

Step 3: Artifact Removal

Based on the preliminary inspection stage, one can proceed to remove the various artifacts. The techniques described in this chapter are most relevant to artifacts that are sufficiently periodic, such as cardiac/respiratory artifacts, 60-Hz and other frequency-localized noise, such as building/fan vibrations.

The fundamental operation is performed on an individual time series. This may be performed pixel by pixel in the image, or to reduce computational time, the steps may

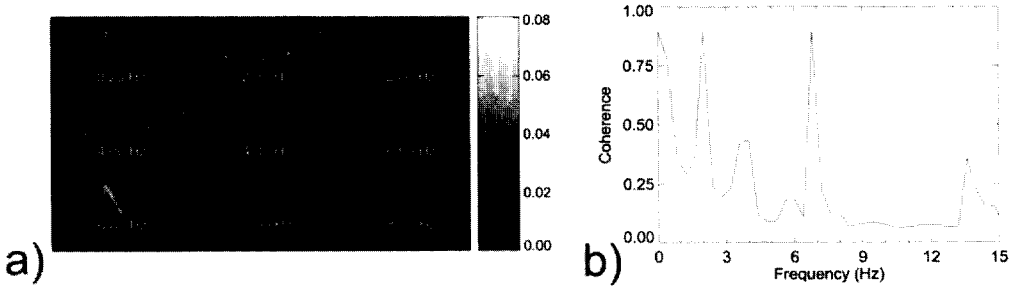

Figure 9.2. Space-frequency SVD of optical imaging data from rat somatosensory cortex. (*a*) The amplitude of the dominant eigenimages as function of center frequency. The respiratory rhythm appears as a spatial derivative highlighting the blood vessels at 2 Hz and harmonics. The cardiac rhythm appears as an increase in luminescence on the vessel at 6.8 Hz. At intermediate frequencies, spatial structure is diminished. (*b*) Overall coherence for the eigenimages in part *a*.

alternatively be performed on the leading principal component (PC) time series and the artifacts thus reconstructed may be then subtracted from the raw data. In the example presented above (see Figure 9.1), the fundamental frequency tracks were adequately extracted from the PC time series. Alternatively, monitored cardiac and respiratory time courses may be used for this purpose.

Step 4: Stimulus Response Characterization

This may be the most delicate step, because the goal of the experiment is usually to find the stimulus response, which is not known a priori. If the stimulus is presented periodically and/or repeatedly, as is usually the case, the characterization of stimulus response is fairly straightforward. However, coherent activity related to a single presentation of the stimulus may be efficiently extracted by the space-frequency SVD technique if the stimulus response is known a priori to inhabit a particular frequency band (including a low-frequency band). An example of the use of this technique may be found in Prechtl et al. (1997) where the phases of the complex SVD eigenmodes were used to obtain a description of the stimulus response in terms of multiple traveling waves of activity.

REFERENCES

Grinvald A., Lieke E.E., Frostig R.D., Gilbert C.D., and Wiesel T.N. 1986. Functional architecture of cortex revealed by optical imaging of intrinsic signals. *Nature* **73:** 2072–2093.

Kleinfeld D. and Delaney K. 1996. Distributed representation of vibrissa movement in the upper layers of somatosensory cortex revealed with voltage sensitive dyes (erratum [1997] **378:** 594). *J. Comp. Neurol.* **375:** 89–108.

Mann M.E. and Park J. 1994. Global-scale modes of surface temperature. *J. Geophys. Res. Atmos.* **99:** 25819–25833.

Mayhew J., Askew S., Zheng Y., Porrill J., Westby G., Redgrave P., Rector D., and Harper R. 1996. Cerebral vasomotion: 0.1 Hz oscillation in reflected light imaging of neural activity. *NeuroImage* **4:** 183–193.

Mitra P.P. and Pesaran B. 1999. The analysis of dynamic brain imaging data. *Biophys. J.* **76:** 691–708.

Mitra P.P., Ogawa S., Hu X.P., and Ugurbil K. 1997. The nature of spatiotemporal changes in cerebral hemodynamics as manifested in functional magnetic resonance imaging. *Magn. Reson. Med.* **37:** 511–518.

Percival D.B. and Walden W.T. 1993. *Spectral analysis for physical applications: Multitaper and conventional univariate techniques.* Cambridge University Press, Cambridge, United Kingdom.

Prechtl J., Cohen L.B., Pesaran B., Mitra P.P., and Kleinfeld D. 1997. Visual stimuli induce waves of electrical activity in turtle cortex. *Proc. Natl. Acad. Sci.* **94:** 7621–7626.

Thomson D.J. 1982. Spectrum estimation and harmonic analysis. *Proc. IEEE* **70:** 1055–1096.

Thomson D.J. and Chave A.D. 1991. Jackknifed error estimates for spectra, coherences, and transfer functions. In *Advances in spectrum analysis and array processing* (ed. S. Haykin), vol. 1, pp. 58–113. Prentice-Hall, Englewood Cliffs, New Jersey.